

Copper Oxide Nanoparticles: Synthesis, Characterization, and Their Biological Effects on Microbial and Cancer Cells

Mosleh Mohammad Abomughaid

Medical Laboratory Sciences Department, College of Applied Medical Sciences, University of Bisha, Bisha 67714, Saudi Arabia

ABSTRACT

Nanomaterials applications in diverse fields are growing annually. The present study aimed to synthesize copper oxide nanoparticles (CuO NPs) and assess their biological impact on microbial and cancer cells. Synthesized nanoparticles are characterized using Fourier Transform Infra-Red (FTIR), Atomic force microscopy (AFM) and Scanning electron microscopy (SEM). Anti-microbial performed using gram-positive, gram-negative, and fungal species. A549 cells was used for anti-cancer studies. The UV visible spectra of the reaction mixture showed a peak at 308 nm, and it represents the copper oxide nanoparticles that have been synthesized. The FTIR analysis of CuO NPs showed the absorbance range between 422.38 cm^{-1} to 3673.18 cm^{-1} . This range reveals the presence of alkyl halides, aliphatic amines, nitro compounds, alkenes, aldehydes, alcohols, and phenols, respectively. AFM and SEM enables precise three-dimensional and two-dimensional mapping of the Copper oxide nanoparticle, the size of the CuO NPs was found to be 7.33 nm. CuO NPs shows dose dependent effect on these Gram-negative, Gram-positive bacteria and fungi. MTT assay was used for the determination of cell viability in A549 lung cancer cells. The IC_{50} was found to be 44.33 $\mu\text{g/ml}$. CuONPs induces reactive oxygen species (ROS) in a dose dependent manner in A549 cells. Presence of apoptotic cells was determined by staining the Annexin V/PI staining. A549 cells treated with CuO NPs, showed the apoptotic body formation. The synthesized CuONPs shows anti-bacterial effect against human bacterial pathogens and anti-fungal effects. Further, CuONPs showed anticancer effect by inhibiting the cell viability of A549 lung cancer cells by increasing ROS and inducing apoptosis. The synthesized CuONPs showed anti-bacterial, anti-fungal and anti-cancer effects.

Article Information

Received 18 March 2024

Revised 10 July 2024

Accepted 24 July 2024

Available online 31 October 2024
(early access)

Key words

CuO NPs, A549 cells, AFM, Nanoparticles

INTRODUCTION

Nanoparticles are crucial in several applications within the field of nanotechnology due to their exceptional qualities, including as enhanced electrical conductivity, mechanical strength, magnetic characteristics, and thermal capabilities, surpassing those of bulk materials (Khan *et al.*, 2021). It can possess desired physical attributes in the fields of materials science and biology, such as uniformity, conductivity, or specialized optical properties. Particles that are nanosized, meaning they have dimensions less than a few tens of nanometers, are highly intriguing.

This is because their chemical and physical characteristics are significantly distinct from those in larger quantities, mostly due to the quantum size effect. As a result, these particles have a broad variety of potential uses (Borghain *et al.*, 2000). The domains of electronics, chemistry, and mechanics, together with related technologies encompassing catalysts, drug carriers, sensors, pigments, and magnetic and electronic materials (Häfeli *et al.*, 2009).

Metal oxide nanoparticles (NPs) are very intriguing due to their exceptional properties, including copper, zinc, titanium, iron, tin, and other elements (McNamara and Tofail, 2017; Chavali and Nikolova, 2019; Nikolova and Chavali, 2020). Copper has a wide range of antibacterial characteristics that are effective against a variety of microorganisms (Alswat *et al.*, 2017; Chen *et al.*, 2021). This phenomenon has the potential to be utilized for therapeutic advantages. However, it is important to note that it might also have negative effects on the symbiotic bacteria present in the environment, skin, or intestines (i.e., the microbiome). Therefore, comprehending the interaction between copper and microorganisms holds significant importance (Vincent *et al.*, 2016).

* Corresponding author: moslehali@ub.edu.sa, mabomughaid@gmail.com
0030-9923/2024/0001-0001 \$ 9.00/0



Copyright 2024 by the authors. Licensee Zoological Society of Pakistan.

This article is an open access article distributed under the terms and conditions of the Creative Commons Attribution (CC BY) license (<https://creativecommons.org/licenses/by/4.0/>).

Cancer is a leading cause of death globally and is characterized by the abnormal proliferation of cells. The World Health Organization reported that over 25 million people globally are affected each year (Soerjomataram and Bray, 2021). The current methods employed in cancer treatment include chemotherapy, immunotherapy, radiation, and surgery (Miller *et al.*, 2019). In recent decades, there has been substantial progress in the field of cancer nanomedicine, resulting in an enhanced therapeutic effectiveness of cancer medications (Gonzalez-Valdivieso *et al.*, 2021; Rasool *et al.*, 2022). Nanotechnology is widely used in the field of biomedical sciences, namely in cancer therapies (Song *et al.*, 2019). Nanomaterials provide significant benefits due to their expansive surface area and diminutive particle size, rendering them highly suitable for the synthesis of medicinal formulations (Shende and Gupta, 2020; Fan *et al.*, 2021).

There is an urgent need for new and innovative therapeutic techniques using nanoparticle medicine systems to improve the treatment and diagnosis of primary and metastatic lung cancers. These tactics aim to reduce unwanted side effects and increase patient survival rates (Chaft *et al.*, 2021). The combination of nanoscience and photodynamic therapy (PDT) offers a promising avenue for the research and advancement of functionalized nanoparticles (NPs) in targeted drug delivery to cancer cells. This approach aims to minimize the impact on healthy cells and enhance patient survival by improving selectivity and specificity (Pallavi *et al.*, 2022). The bioactive uses of CuO NPs have garnered significant attention due to their multifunctional characteristics, including catalysis, photoconductivity, and photothermal and biocidal effects (Shanan *et al.*, 2018; Saravanakumar *et al.*, 2019). Various studies have concentrated on diverse varieties of metal oxide NPs, which are extensively employed for the purpose of treating cancer cells. Phull *et al.* (2021) found that CuONPs produced copper ions, leading to DNA damage, cell cycle arrest, and inhibition of cell proliferation in cervical cancer HeLa cells (Phull *et al.*, 2021). Singh *et al.* (2022) and Elsayed *et al.* (2021) have shown the successful use of green produced modified CuONPs in the treatment of breast cancer, demonstrating their potent anticancer characteristics (Elsayed *et al.*, 2021; Singh *et al.*, 2022). This work involved the synthesis of CuONPs synthesized by chemical precipitation method and the evaluation of its anti-bacterial activity against Gram-negative and Gram positive clinical bacterial pathogens. In this study, we evaluated the anticancer effect of CuO NPs in lung cancer cells by inducing reactive oxygen species (ROS) and apoptosis.

MATERIALS AND METHODS

Preparation of copper oxide nanoparticles

To synthesize CuONPs, 2.9 g of copper nitrate and 1.2 g of polyvinylpyrrolidone (PVP) were dissolved in 100 ml of distilled water using a magnetic stirrer and heated to a temperature of 600 °C. After that, 1M NaOH was gradually added drop by drop heated and agitated for one hour till black precipitate appeared which was subjected to centrifugation and then dried in an oven at a temperature of 500 °C for a duration of 2 h. This CuONPs solution has a pH of 10.5 (Luna and Commission, 2015).

Fourier transform infra-red (FTIR)

The copper oxide was preceded for the identification of functional groups by using FTIR Spectrometer (Nicolet™ iS20) (Thermo Fisher Scientific, Madison, USA). The synthesized CuO NPs samples can be liquid, solid, or gaseous. The analysis region on a spectrometer with a microscope attachment can be as small as 10 µm. The reflectance model of the microscope can be used to investigate thin organic coatings on a reflecting surface (such as CuO NPs). A material exterior 1-10 µm can be studied using attenuated total reflectance (ATR). The unknown IR absorption spectrum is compared to standard spectra in computer databases, or a spectrum derived from a known substance to identify the material under investigation. The polymer or other constituent(s) in the sample can be identified using spectrum matching. Wave numbers range from 1500 to 400 while absorption bands span from 4000 to 1500.

Ultraviolet (UV) analysis

UV-Vis spectrophotometer (GENESYS™ 150) (Thermo Fisher Scientific, Madison, USA) was used to analyze the UV spectrum of the synthesized copper oxide nanoparticles. The synthesized CuO NPs are observable within the visible spectrum, which spans from 400 to 700 nm, and the UV band, which spans from 100 to 400 nm. The term “Deep UV” specifically denotes the wavelength region between 100 and 200 nm. The confirmation of the CuO NPs synthesis was achieved using a 200 nm measurement (Jadhav *et al.*, 2011).

Atomic force microscopy and scanning electron microscopy

The 5 µl sample was placed onto newly cleaved ASTM V1 Grade Mica from MICAFAFAB for a duration of 15-30 min. Mica sheets possess a negative charge, which results in a strong binding of nanomaterials to the mica surface within a 15-min time frame. The AAC mode AFM was conducted using an Agilent Technologies Pico plus 5500 ILM AFM from the USA, equipped with a piezo

scanner that has a maximum range of 9 μm . In the United States, nano sensors supplied microfabricated silicon cantilevers with a spring force constant of 2198 N/m. The oscillation frequency of the cantilever was adjusted to match its resonance frequency. The cantilever resonance occurred at a frequency range of 150-300 kHz. The images (256 \times 256 pixels) were acquired at a scanning rate of 0.5 lines per second, with a scanning range of 0.5 to 5 mm. The photos were flattened using the Pico view 1.1 version software from Agilent Technologies, USA.

The particle size and surface morphology of the produced nanoparticles were analyzed using the Carl Zeiss Ultra Plus Field-Emission Scanning Electron Microscope, a type of microscope that utilizes field emission scanning electron microscopy. The sample was deposited onto a carbon-coated copper grid by applying a tiny quantity of the sample onto the grid. The coated CuO nanoparticles were examined using a high vacuum of 12 kV. The FE-SEM pictures and size distribution of the CuO NPs were examined using Image 1.46r software (Jadhav *et al.*, 2011).

Antibacterial and antifungal activities

Bacteria and fungi used in the present study was purchased from ATCC. The synthesized nanoparticles, as well as the standard solution, were dissolved in DMSO, and the procedure was carried out in four-well plates on Muller Hinton agar (Cat No: 70191, Sigma, USA). Then 15 μL of compound (in sterile form) was injected into the well, and the extract was allowed to dry for several min while the disc was kept on the plate surface followed by incubation at 37 $^{\circ}\text{C}$. The human clinical pathogens were selected for this study namely, *Escherichia coli*, *Proteus vulgaris*, *Streptococcus pneumoniae*, *Enterococcus faecalis*, *Pseudomonas aeruginosa* and *Shigella flexneri*. Chloramphenicol was used as a positive control; ammonium chloride was used as a negative control. For anti-fungal studies, fungal cultures like *Candida albicans*, *Aspergillus flavus* and *Penicillium chrysogenum* were spread on the sabouraud dextrose agar (Cat No: 84088, Sigma, USA) using sterile cotton swab. Amphotericin B was used as a positive control and ammonium chloride was used as a negative control. Sterile nanoparticle 30 μg solution was injected into the wells that created in the petri plate. The plates were kept at 32 $^{\circ}\text{C}$ for a week to allow the fungi to grow (Jadhav *et al.*, 2011).

Determination of minimum inhibitory concentration (MIC)

The MIC tests were carried out in nutritional broth (Cat No: 70122, Sigma, USA) included with various doses of CuO NPs and inoculated with the test microorganisms. The 0.1 ml of each culture was distributed on nutritional agar plates and incubated at 37 $^{\circ}\text{C}$ for 24 h. Then CFU/

mL in control plates was compared to CFU/mL in each NPs supplemented plate. All experiments were done three times, and the averages were calculated.

MTT assay

The A549 cell line, derived from human lung cancer cells, was acquired from ATCC, short tandem repeat (STR) test was performed to confirm the authentication and checked for mycoplasma contamination. All the experiments were done using 5-10 cell passage. The cells were cultured in Dulbecco's Modified Eagle's Medium (DMEM) (Sigma, USA) supplemented with 10% fetal bovine serum (FBS), 100 $\mu\text{g}/\text{ml}$ penicillin, and 100 g/ml streptomycin (Sigma, USA). The culture was maintained at a temperature of 37 $^{\circ}\text{C}$ in an atmosphere with 5% CO_2 . The *in vitro* cytotoxicity of the sample was assessed using the MTT test with A549 cells. The process of trypsinization was used to gather the cultured A549 cells, which were subsequently mixed in a 15 ml tube. The cells were subsequently distributed into a 96-well tissue culture plate, with each well containing 200 μL of cells at a concentration of 1×10^4 cells/ml in DMEM medium supplemented with 10% FBS and 1% antibiotic solution. The plate was then incubated at 37 $^{\circ}\text{C}$ for 48 h. The wells were washed with sterile PBS and then exposed to different concentrations (1, 5, 10, 15, 50, 100, 200, 300, 400, and 500 $\mu\text{g}/\text{mL}$) of the experimental material (CuO NPs) in a serum-free DMEM medium. Every assay was performed in triplicate, with the cells cultivated for 24 h at 37 $^{\circ}\text{C}$ in a humidified incubator with 5% CO_2 . Following the incubation time, 20 μL of MTT (Sigma, USA) solution with a concentration of 5 mg/ml was introduced into each well. The cells were then incubated for a further 2-4 h until the formation of purple precipitates, which could be observed using an inverted microscope. Ultimately, the liquid in the wells was removed and washed with 1X PBS (200 μL). In addition, 100 μL of DMSO was used to dissolve the formazan crystals, and the plate was stirred for a duration of 5 min. The absorbance of each well was measured at 570 nm using a microplate reader from Thermo Fisher Scientific, USA. The GraphPad Prism 6.0 software was used to calculate the % cell viability and IC_{50} value (Phull *et al.*, 2021).

Cell viability of the treatment group was calculated using formula below:

$$\text{Cell viability (\%)} = \frac{\text{OD570 treatment}}{\text{OD570 control}} \times 100$$

ROS assay

ROS generated in A549 cells treated with CuO NPs was evaluated using a fluorescent probe 2, 7-dichlorofluorescein diacetate (DCHF-DA) (Sigma,

USA). A549 cells were seeded at a density of 1×10^5 cells/well. Cells were incubated with $10 \mu\text{M}$ of DCFH-DA and incubated for 30 Min, followed by CuO NPs treatment with different concentrations (10, 50, 100, 250 and $500 \mu\text{g}/\text{mL}$). H_2O_2 is used as a positive control. Then the cells were harvested, centrifuged, washed, and resuspended in PBS and read in a Hitachi spectrofluorometer using excitation/emission as 480/520 nm (Baskaran *et al.*, 2016).

Annexin V/ propidium iodide apoptosis staining assay

A549 cells were seeded in 96-well tissue culture plates at a density of 5×10^5 cells/ml. The wells were washed with sterile PBS and then exposed to a concentration of $44.33 \text{ g}/\text{ml}$ of CuO NPs sample in a serum-free DMEM medium. The plate was incubated at a temperature of 37°C in a CO_2 incubator with a concentration of 5% for a duration of 24 h. After the incubation period, $10 \mu\text{l}$ of Alexa Fluor 488 annexin v and $10 \mu\text{l}$ of propidium iodide (PI) were introduced into the wells and mixed gently. The mixture was then incubated for 15 min. Subsequently, $400 \mu\text{l}$ of 1x Annexin binding buffer was added and delicately blended. Ultimately, the plate underwent centrifugation at a speed of 800 rpm for a duration of 2 min. Subsequently, the cells were examined utilizing a fluorescence microscope equipped with a fluorescent filter, all inside a time frame of one hour (Baskaran *et al.*, 2016).

Statistical analysis

SPSS software version 22 (Chicago, IL, USA) was used for various steps of data analysis. All experimental data were expressed as mean \pm SD. Statistical analysis was performed by one-way analysis of variants. $p < 0.05$ was considered statistically significant.

RESULTS

Characteristics of prepared CuONPs

An ultraviolet-visible spectrum of CuO nanoparticles was identified by UV visible spectroscopy. The scan distance range was set between 200 and 800 nm. Figure 1 shows the UV visible spectra of the reaction mixture showed the peak at 308 nm, and it represents the synthesis of CuO nanoparticles.

The copper oxide was preceded for the identification of functional groups by using FTIR Spectrometer (Nicolet™ iS20) (Thermo Fisher Scientific, Madison, USA). It showed the absorbance range between 422.38 cm^{-1} to 3673.18 cm^{-1} . The peaks denote the presence of the following compounds, namely alkyl halides, aliphatic amines, nitro compounds, alkenes, aldehydes, alcohols, and phenols, respectively. The infrared (IR) spectra of synthesized samples of CuONPs are shown in Figure 2.

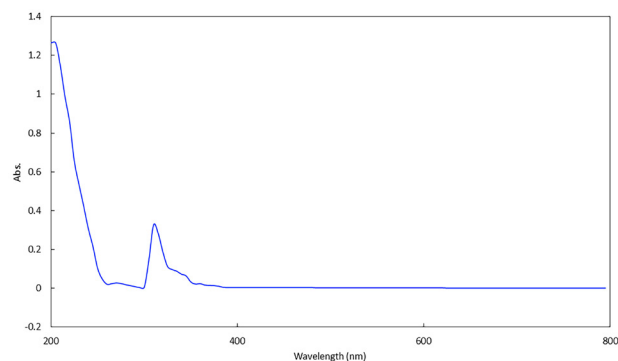


Fig. 1. UV Visible spectroscopy of synthesized CuONPs.

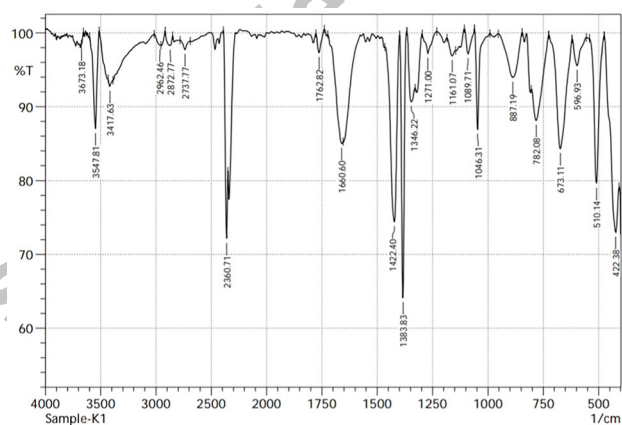


Fig. 2. FT-IR spectrum representing the functional groups of synthesized CuONPs.

Characteristic peaks of IR spectra are in the range of $500\text{--}4000 \text{ cm}^{-1}$. Cu-O stretching was found at 510 and 595 cm^{-1} in the FTIR spectra of CuO from classical chemical production. The peak observed at 3673 cm^{-1} is associated with OH stretching present as a result of the hydroxyl group on the surface of the CuO (Supplementary Table 1). Each molecule produced a unique spectrum, to identify the unique chemical groups in which it is used to know the functional group and the compound class of synthesized nanoparticles. The results showed some major peak values like 510.14, 596.93, 673.11, 782.08, 887.19, 1046.31, 1089.71, 1161.07, 1271, 1346.22, 1383.83, 1422.4, 1660.6, 1762.82, 2360.71, 2737.77, 2872.77, 2962.46, 3417.63, 3547.81, 3645.18 cm^{-1} which signify various functional groups, like alkyl halides, 1°, 2° amines, aliphatic amines, nitro compounds, alkenes, aldehydes, alkanes, aromatics, carbonyls, nitriles, alcohols and phenols.

Nano images of the CuONPs were observed in the Atomic Force Microscopy (AFM) which provided precise three-dimensional and two-dimensional mapping of the

CuO NPs (Fig. 3A). Due to its high-resolution capabilities, AFM was limited to a confined measuring range (XYZ). As a result, the nanoparticles were determined to be 7.33 nm.

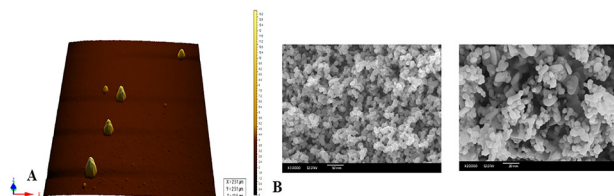


Fig. 3. (A) AFM analysis of three-dimensional image showing the topology and distribution characteristics of synthesized CuO NPs. (B) FE-SEM analysis of CuO NPs.

Figure 3B shows the scanning electron microscopic images of the synthesized CuONPs. The results are FE-SEM represented in uniform distribution and spherical shape of the CuONPs. Furthermore, the average particle size was observed to be 8 nm.

Antibacterial activity of CuONPs

Gram-negative bacteria, such as *Escherichia coli*, *Proteus vulgaris*, *Pseudomonas aeruginosa* and *Shigella flexneri* showed 20.42, 22.53, 7.52, and 11.72 mm inhibition at 500 $\mu\text{g}/\text{mL}$ concentration, respectively (Fig. 4A). Gram-positive bacteria, *Streptococcus pneumoniae*, and *Enterococcus faecalis* showed 19.35 and 19.53 mm inhibition at 500 $\mu\text{g}/\text{mL}$ concentration, respectively (Fig. 4B). At lower CuO NPs (10 $\mu\text{g}/\text{mL}$) concentration the zones of inhibition were found to be 2.21, 1.93, 1.53, 1.78, 3.02 and 2.76 mm for *Escherichia coli*, *Proteus vulgaris*, *Pseudomonas aeruginosa*, *Shigella flexneri*, *Streptococcus pneumoniae*, and *Enterococcus faecalis*, respectively.

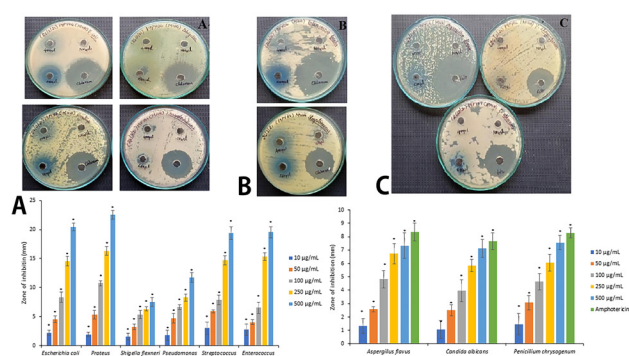


Fig. 4. Antibacterial activity CuONPs against Gram-negative bacteria (A); Gram-positive bacteria (B) and antifungal activity (C) of CuONPs. * $p < 0.05$ compared to control.

Antifungal activity of CuONPs

The anti-fungal activity of the synthesized CuO NPs was tested against three different fungi, including *Candida albicans*, *Aspergillus flavus* and *Penicillium chrysogenum* and was compared to the conventional medications of Amphotericin B. At 500 $\mu\text{g}/\text{mL}$, synthesized CuO-NPs demonstrated greater action against *C. albicans*, *A. flavus* and *Penicillium* sp. (Fig. 4C).

Effect of CuONPs against A549 lung cancer cells

To evaluate the effect of synthesized CuO NPs *in vitro*, we used a A549 cancer cells. The A549 cells were treated with different concentration of CuO NPs (1, 5, 10, 15, 50, 100, 200, 300, 400 and 500 $\mu\text{g}/\text{mL}$) and the cellular toxicity was determined. The cell viability was found to be 43.04, 47.39, 48.99, 53.23, 63.60, 68.40, 77.18, 87.20, 91.79, and 95.65%, respectively. The cell viability was significantly reduced gradually from 5 $\mu\text{g}/\text{mL}$ when compared to the control (Fig. 5A). IC_{50} values, the inhibitory concentration of CuO NP was found to be 44.33 $\mu\text{g}/\text{mL}$.

The impact of *in vitro* produced CuO NPs on cancer line cells (A549 cells) was determined in under the various concentrations (100, 200, 300, 400 and 500 $\mu\text{g}/\text{mL}$) at 570 nm. The morphological changes after CuO NPs treatment in the A549 was observed using the microscope and it shows the results of various concentration ranges from 500, 300, 100, 50, 10, and 1 $\mu\text{g}/\text{mL}$ (Fig. 5B).

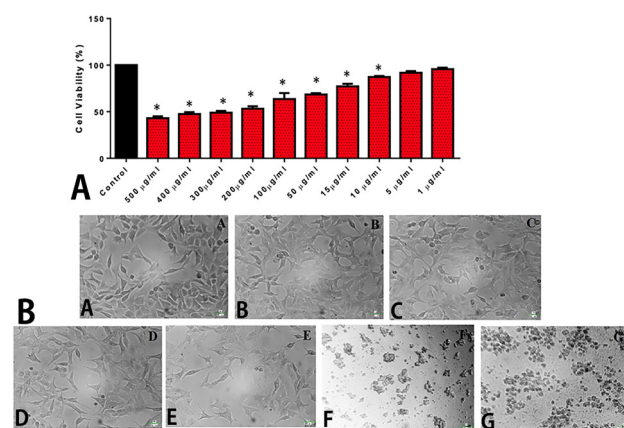


Fig. 5. (A) Effect of CuONPs on A549 cell viability (%) using MTT assay. (B) Phase contrast microscopic image of the A549 cells treated with different concentrations of CuO NP. (a) Control, (b) 1 $\mu\text{g}/\text{mL}$, (c) 10 $\mu\text{g}/\text{mL}$, (d) 50 $\mu\text{g}/\text{mL}$, (e) 100 $\mu\text{g}/\text{mL}$, (f) 300 $\mu\text{g}/\text{mL}$, (g) 500 $\mu\text{g}/\text{mL}$. * $p < 0.05$ compared to control.

Effect of CuO NPs on ROS generation in A549 cells

Studying the prevention of ROS formation within cancer cells is crucial, since it is a result of oxidative stress

responses induced by the treated material. The exposure of A549 cells to CuO NPs leads to the production ROS in a way that is dependent on the dosage. Cells treated with H_2O_2 also induces the production of ROS (Fig. 6). The findings of our study indicate that the synthesized CuONPs possess an anti-cancer impact through the stimulation of ROS production.

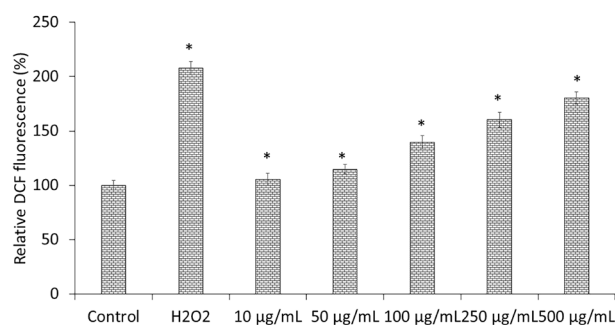


Fig. 6. Effect of CuONPs on ROS generation in A549 lung cancer cells. * $p < 0.05$ compared to control.

Annexin V/PI apoptosis staining assay

Apoptotic activity of the in vitro synthesized CuO NPs on the cancer cell line (A549) was determined using annexin V marker and PI. The apoptotic bodies were seen using a fluorescent microscope (Fig. 7). The CuO NPs sample exhibited an IC_{50} value of $44.33 \mu\text{g/ml}$. The presence of apoptotic cells was assessed by Annexin V/PI staining. The cells exposed to fluorouracil exhibited a mixture of viable and non-viable cells, whereas those treated with CuO NPs showed the presence of apoptotic bodies. Living cells emitted green fluorescence, whereas dead cells displayed red fluorescence, with early apoptotic cells exhibiting yellow reflection in the cultured cells.

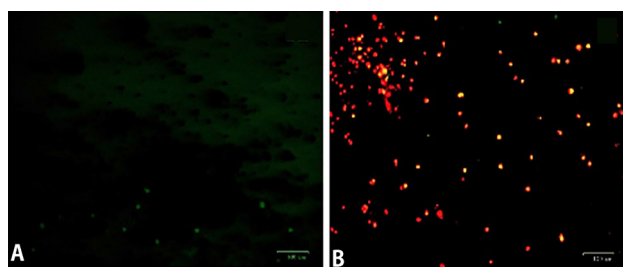


Fig. 7. Annexin V/PI apoptosis staining assay for detecting apoptotic bodies formation in A549 cells. (A) Control, (B) $44.33 \mu\text{g/ml}$ CuO NP.

DISCUSSION

The synthesis of CuONPs was carried out in manual

method, and the brownish-black colored solution is formed by using chemicals and then it was dried as powder using oven-dry at 50°C for two hour to get copper oxide nano powder. Similar to previous studied by Sagadevan *et al.* (2019) a peak at 308 nm is also visible in the present UV examination. Followed by Jadhav *et al.* (2011) the absorption spectra for the sample were obtained between the wavelength ranges of 200 and 800 nm.

In the present study reveals the CuONPs characterized for the identification of functional groups using FTIR as was previously done by Prakash *et al.* (2018) for copper and zinc oxide NPs. The structural characterization of the synthesized NPs was done by AFM and SEM (Rheima *et al.*, 2020). Likewise, by this AFM technique, the height of the CuO nanoparticle was found to be 7.33 nm.

The antimicrobial activity of CuONPs was determined against human pathogen. It was found that Gram-positive bacteria had higher antibacterial effect than Gram-negative bacteria. A previous finding has reported MIC values that were slightly higher than others findings (Ren *et al.*, 2009; Meghana *et al.*, 2015; Amiri *et al.*, 2017; Sasidharan *et al.*, 2020). Ahmad *et al.* (2020) reported that the anti-fungal activity of CuO-NPs synthesized using *A. indica* was determined against three plant pathogenic fungi viz., *Alternaria mali*, *Diplodia seriata* and *Botryosphaeria dothidea* dominant in apple orchards of Kashmir valley in India (Ahmad *et al.*, 2020).

The goal of this study was to see how CuONPs affected the proliferation of A549 human lung cancer cell line. The cell viability in growth concentration is $1 \mu\text{g/ml}$ and in mean value are 95.65 and decrease the concentration value for $500 \mu\text{g/ml}$ in mean value are 43.04 for triplicates for cell viability. The potential cytotoxicity of CuO-NPs has been found to be 4.99 and $3.75 \mu\text{g/ml}$ in HT-29 and SW620 cancer cell lines (Khan *et al.*, 2017), respectively (Khan *et al.*, 2017).

Ag NPs treated at a higher concentration to A549 cells stimulate the production of ROS (Tian *et al.*, 2020). Furthermore, because of internal leaks in the mitochondrial membrane, the oxidative stress response also moved to down-regulate the process in apoptotic genes and causes programmed cell death (Tian *et al.*, 2020). In the present study, the anticancer activity was examined using CuONPs by apoptosis with cancer cell. CuONPs using human cell lines and identified the targeted cells by apoptosis detection methods with reference to MTT assay. CuONPs have the specific capability leads to oxidative stress in most cancer cells, which has been observed that the mechanisms of cytotoxicity of CuONPs against most cancer cells (Khan *et al.*, 2017). In a similar manner, Pandurangan *et al.* (2016) observed that the AgNPs triggered apoptosis in HeLa cells. The researchers examined this phenomenon using

fluorescence and confocal microscopes for a duration of 48 and 72 h. The hundred cells were enumerated for both the control group and each concentration level. The fluorescent microscope revealed that the proportion of apoptotic cells in samples treated with AgNP at concentrations of 0.01, 0.02, and 0.04 mg/ml was 42%, 51%, and 55%, respectively. In comparison, the percentage of apoptotic cells in untreated samples was 54%, 60%, and 62%, respectively (Pandurangan *et al.*, 2016). Hsin *et al.* (2008) observed that apoptosis is distinguished by both morphological and biochemical alterations. Furthermore, they found that cells within the same tissue undergo apoptosis at distinct time intervals. Early-stage apoptosis studies rely heavily on morphological observations due to the ability to visually detect DNA replication following the beginning of apoptosis. The apoptotic impact of AgNPs was documented through experimentation on mouse NIH3T3 cells (Hsin *et al.*, 2008). Li *et al.* (2018) found that selenium NPs had a direct impact on the morphology of MDCK cells, and this effect was dependent on the dosage of selenium NPs. A morphological observation was conducted to see if there was a correlation between the cytotoxic impact of selenium NPs and the apoptotic process (Li *et al.*, 2018).

CONCLUSION

Nanomaterials applications in diverse fields are growing annually. The synthesized CuO NPs shows anti-bacterial effect against human bacterial pathogens and anti-fungal effect against fungi. Further, CuO NPs showed anticancer effect by inhibiting the cell viability of A549 lung cancer cells by inducing apoptosis. The synthesized CuO NPs showed anti-bacterial, anti-fungal and anti-cancer effects.

DECLARATIONS

Acknowledgements

The author is grateful to the Deanship of Graduate Studies and Scientific Research at University of Bisha for supporting this work through the Fast-Track Research Support Program.

Funding

No Funding received for this study.

Supplementary material

There is supplementary material associated with this article. Access the material online at: <https://dx.doi.org/10.17582/journal.pjz/20240318172852>

Statement of conflicts of interest

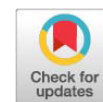
The authors have declared no conflict of interest.

REFERENCES

- Ahmad, H., Venugopal, K., Bhat, A., Kavitha, K., Ramanan, A., Rajagopal, K., Srinivasan R. and Manikandan, E., 2020. Enhanced biosynthesis synthesis of copper oxide nanoparticles (cuo-nps) for their antifungal activity toxicity against major phyto-pathogens of apple orchards. *Pharma. Res.*, **37**: 1-12. <https://doi.org/10.1007/s11095-020-02966-x>
- Alswat, A.A., Ahmad, M.B., Hussein, M.Z., Ibrahim, N.A. and Saleh, T.A., 2017. Copper oxide nanoparticles-loaded zeolite and its characteristics and antibacterial activities. *J. Mat. Sci. Technol.*, **33**: 889-896. <https://doi.org/10.1016/j.jmst.2017.03.015>
- Amiri, M., Etemadifar, Z., Daneshkazemi A. and Nateghi, M., 2017. Antimicrobial effect of copper oxide nanoparticles on some oral bacteria and candida species. *J. Dent. Biomat.*, **4**: 347.
- Baskaran, R., Poornima, P., Huang C.Y. and Padma, V.V., 2016. Neferine prevents nf-kb translocation and protects muscle cells from oxidative stress and apoptosis induced by hypoxia. *Biofactors*, **42**: 407-417. <https://doi.org/10.1002/biof.1286>
- Borghain, K., Singh, J.B., Rao, M.R., Shripathi, T. and Mahamuni, S., 2000. Quantum size effects in cuo nanoparticles. *Phys. Rev. B*, **61**: 11093. <https://doi.org/10.1103/PhysRevB.61.11093>
- Chaft, J.E., Rimmer, A., Weder, W., Azzoli, C.G., Kris, M.G. and Cascone, T., 2021. Evolution of systemic therapy for stages i-iii non-metastatic non-small-cell lung cancer. *Nat. Rev. Clin. Oncol.*, **18**: 547-557. <https://doi.org/10.1038/s41571-021-00501-4>
- Chavali, M.S. and Nikolova, M.P., 2019. Metal oxide nanoparticles and their applications in nanotechnology. *SN appl. Sci.*, **1**: 607. <https://doi.org/10.1007/s42452-019-0592-3>
- Chen, N.F., Liao, Y.H., Lin, P.Y., Chen, W.F., Wen, Z.H. and Hsieh, S., 2021. Investigation of the characteristics and antibacterial activity of polymer-modified copper oxide nanoparticles. *Int. J. mol. Sci.*, **22**: 12913. <https://doi.org/10.3390/ijms222312913>
- Elsayed, A.M., Sherif, N.M., Hassan, N.S., Althobaiti, F., Hanafy, N.A. and Sahyon, H.A., 2021. Novel quercetin encapsulated chitosan functionalized copper oxide nanoparticles as anti-breast cancer agent via regulating p53 in rat model. *Int. J. biol.*

- Macromol.*, **185**: 134-152. <https://doi.org/10.1016/j.ijbiomac.2021.06.085>
- Fan, Y., Marioli, M. and Zhang, K., 2021. Analytical characterization of liposomes and other lipid nanoparticles for drug delivery. *J. Pharma. Biomed. Anal.*, **192**: 113642. <https://doi.org/10.1016/j.jpba.2020.113642>
- Gonzalez-Valdivieso, J., Girotti, A., Schneider, J. and Arias, F.J., 2021. Advanced nanomedicine and cancer: Challenges and opportunities in clinical translation. *Int. J. Pharma.*, **599**: 120438. <https://doi.org/10.1016/j.ijpharm.2021.120438>
- Häfeli, U.O., Riffle, J.S., Harris-Shekhawat, L., Carmichael-Baranauskas, A., Mark, F., Dailey, J.P. and Bardenstein, D., 2009. Cell uptake and *in vitro* toxicity of magnetic nanoparticles suitable for drug delivery. *Mol. Pharmacol.*, **6**: 1417-1428. <https://doi.org/10.1021/mp900083m>
- Hsin, Y.H., Chen, C.F., Huang, S., Shih, T.S., Lai, P.S. and Chueh, P.J., 2008. The apoptotic effect of nanosilver is mediated by a ros-and jnk-dependent mechanism involving the mitochondrial pathway in nih3t3 cells. *Toxicol. Lett.*, **179**: 130-139. <https://doi.org/10.1016/j.toxlet.2008.04.015>
- Jadhav, S., Gaikwad, S., Nimse, M. and Rajbhoj, A., 2011. Copper oxide nanoparticles: Synthesis, characterization and their antibacterial activity. *J. Cluster Sci.*, **22**: 121-129. <https://doi.org/10.1007/s10876-011-0349-7>
- Khan, S., Ansari, A.A., Khan, A.A., Abdulla, M., Al-Obaid, O. and Ahmad, R., 2017. *In vitro* evaluation of cytotoxicity, possible alteration of apoptotic regulatory proteins, and antibacterial activity of synthesized copper oxide nanoparticles. *Colloids Surf. B: Biointerf.*, **153**: 320-326. <https://doi.org/10.1016/j.colsurfb.2017.03.005>
- Khan, S., Naushad, M., Al-Gheethi, A. and Iqbal, J., 2021. Engineered nanoparticles for removal of pollutants from wastewater: Current status and future prospects of nanotechnology for remediation strategies. *J. environ. Chem. Engin.*, **9**: 106160. <https://doi.org/10.1016/j.jece.2021.106160>
- Li, Y., Lin, Z., Guo, M., Zhao, M., Xia, Y., Wang, C., Xu, T. and Zhu, B., 2018. Inhibition of h1n1 influenza virus-induced apoptosis by functionalized selenium nanoparticles with amantadine through ros-mediated akt signaling pathways. *Int. J. Nanomed.*, **2018**: 2005-2016. <https://doi.org/10.2147/IJN.S155994>
- Luna, I.Z. and Commission, B.A.E., 2015. Preparation and characterization of copper oxide nanoparticles synthesized via chemical precipitation method. *Open Access Libr. J.*, **2**: 1. <https://doi.org/10.4236/oalib.1101409>
- McNamara, K. and Tofail, S.A., 2017. Nanoparticles in biomedical applications. *Adv. Phys. X*, **2**: 54-88. <https://doi.org/10.1080/23746149.2016.1254570>
- Meghana, S., Kabra, P., Chakraborty S. and Padmavathy, N., 2015. Understanding the pathway of antibacterial activity of copper oxide nanoparticles. *RSC Adv.*, **5**: 12293-12299. <https://doi.org/10.1039/C4RA12163E>
- Miller, K.D., Nogueira, L., Mariotto, A.B., Rowland, J.H., Yabroff, K.R., Alfano, C.M., Jemal, A., Kramer, J.L. and Siegel, R.L., 2019. Cancer treatment and survivorship statistics. *CA: A Canc. J. Clin.*, **69**: 363-385. <https://doi.org/10.3322/caac.21565>
- Nikolova, M.P. and Chavali, M.S., 2020. Metal oxide nanoparticles as biomedical materials. *Biomimetics*, **5**: 27. <https://doi.org/10.3390/biomimetics5020027>
- Pallavi, P., Sharmiladevi, P., Haribabu, V., Girigoswami, K. and Girigoswami, A., 2022. A nano approach to formulate photosensitizers for photodynamic therapy. *Curr. Nanosci.*, **18**: 675-689. <https://doi.org/10.2174/1573413718666211222162041>
- Pandurangan, M., Enkhtaivan, G., Venkitesamy, B., Mistry, B., Noorzai, R., Jin, B.Y. and Kim, D.H., 2016. Time and concentration-dependent therapeutic potential of silver nanoparticles in cervical carcinoma cells. *Biol. Trace Elem. Res.*, **170**: 309-319. <https://doi.org/10.1007/s12011-015-0467-4>
- Phull, A.R., Ali, A., Dhong, K.R., Zia, M., Mahajan, P.G. and Park, H.J., 2021. Synthesis, characterization, anticancer activity assessment and apoptosis signaling of fucoidan mediated copper oxide nanoparticles. *Arab J. Chem.*, **14**: 103250. <https://doi.org/10.1016/j.arabjc.2021.103250>
- Prakash, S., Elavarasan, N., Venkatesan, A., Subashini, K., Sowndharya, M. and Sujatha, V., 2018. Green synthesis of copper oxide nanoparticles and its effective applications in biginelli reaction, btb photodegradation and antibacterial activity. *Adv. Powder Technol.*, **29**: 3315-3326. <https://doi.org/10.1016/j.apt.2018.09.009>
- Rasool, M., Malik, A., Waquar, S., Arooj, M., Zahid, S., Asif, M., Shaheen, S., Hussain, A., Ullah, H. and Gan, S.H., 2022. New challenges in the use of nanomedicine in cancer therapy. *Bioengineered*, **13**: 759-773. <https://doi.org/10.1080/21655979.2021.2012907>
- Ren, G., Hu, D., Cheng, E.W., Vargas-Reus, M.A., Reip, P. and Allaker, R.P., 2009. Characterisation of copper

- oxide nanoparticles for antimicrobial applications. *Int. J. Antimicrob. Agents*, **33**: 587-590. <https://doi.org/10.1016/j.ijantimicag.2008.12.004>
- Rheima, A., Anber, A., Shakir, A., Salah-Hammed, A. and Hameed, S., 2020. Novel method to synthesis nickel oxide nanoparticles for antibacterial activity. *Iran. J. Phys. Res.*, **20**: 51-55. <https://doi.org/10.47176/ijpr.20.3.38771>
- Sagadevan, S., Vennila, S., Marlinda, A.R., Al-Douri, Y., Rafie-Johan, M. and Anita-Lett, J., 2019. Synthesis and evaluation of the structural, optical, and antibacterial properties of copper oxide nanoparticles. *Appl. Phys. A*, **125**: 1-9. <https://doi.org/10.1007/s00339-019-2785-4>
- Saravanakumar, K., Shanmugam, S., Varukattu, N.B., MubarakAli, D., Kathiresan, K. and Wang, M.H., 2019. Biosynthesis and characterization of copper oxide nanoparticles from indigenous fungi and its effect of photothermolysis on human lung carcinoma. *J. Photochem. Photobiol. B Biol.*, **190**: 103-109. <https://doi.org/10.1016/j.jphotobiol.2018.11.017>
- Sasidharan, D., Namitha, T., Johnson, S.P., Jose, V. and Mathew, P., 2020. Synthesis of silver and copper oxide nanoparticles using myristica fragrans fruit extract: Antimicrobial and catalytic applications. *Sustain. Chem. Pharm.*, **16**: 100255. <https://doi.org/10.1016/j.scp.2020.100255>
- Shanan, Z.J., Hadi, S.M. and Shanshool, S.K., 2018. Structural analysis of chemical and green synthesis of cuo nanoparticles and their effect on biofilm formation. *Baghdad Sci. J.*, **15**: 0211-0211. <https://doi.org/10.21123/bsj.2018.15.2.0211>
- Shende, P. and Gupta, H., 2020. Formulation and comparative characterization of nanoparticles of curcumin using natural, synthetic and semi-synthetic polymers for wound healing. *Life Sci.*, **253**: 117588. <https://doi.org/10.1016/j.lfs.2020.117588>
- Singh, S., Ghosh, C., Roy, P. and Pal, K., 2022. Biosynthesis of folic acid appended phbv modified copper oxide nanorods for ph sensitive drug release in targeted breast cancer therapy. *Int. J. Pharma.*, **622**: 121831. <https://doi.org/10.1016/j.ijpharm.2022.121831>
- Soerjomataram, I. and Bray, F., 2021. Planning for tomorrow: Global cancer incidence and the role of prevention 2020–2070. *Nat. Rev. Clin. Oncol.*, **18**: 663-672. <https://doi.org/10.1038/s41571-021-00514-z>
- Song, W., Anselmo, A.C. and Huang, L., 2019. Nanotechnology intervention of the microbiome for cancer therapy. *Nat. Nanotech.*, **14**: 1093-1103. <https://doi.org/10.1038/s41565-019-0589-5>
- Tian, S., Saravanan, K., Mothana, R.A., Ramachandran, G., Rajivgandhi, G. and Manoharan, N., 2020. Anti-cancer activity of biosynthesized silver nanoparticles using avicennia marina against a549 lung cancer cells through ros/mitochondrial damages. *Saudi J. Biol. Sci.*, **27**: 3018-3024. <https://doi.org/10.1016/j.sjbs.2020.08.029>
- Vincent, M., Hartemann, P. and Engels-Deutsch, M., 2016. Antimicrobial applications of copper. *Int. J. Hyg. environ. Hlth.*, **219**: 585-591. <https://doi.org/10.1016/j.ijhheh.2016.06.003>



Supplementary Material

Copper Oxide Nanoparticles: Synthesis, Characterization, and Their Biological Effects on Microbial and Cancer Cells

Mosleh Mohammad Abomughaid

Medical Laboratory Sciences Department, College of Applied Medical Sciences,
University of Bisha, Bisha 67714, Saudi Arabia


Supplementary Table 1. Functional groups of CuO nanoparticles revealed by FT-IR analysis.

Peak value (cm ⁻¹)	Bond	Class of Compounds
515.14	C–Br stretch	alkyl halides
596.93	C–Br stretch	alkyl halides
673.11	C–Br stretch	alkyl halides
782.08	N–H wag	1°, 2° amines
887.19	N–H wag	1°, 2° amines
1046.31	C–N stretch	aliphatic amines
1089.7	C–N stretch	aliphatic amines
1161.07	C–N stretch	aliphatic amines
1271	C–H wag (–CH ₂ X)	alkyl halides
1346.22	N–O symmetric stretch	nitro compounds
1383.83	C–H	Alkanes
1422.4	C–C stretch	Aromatics
1660.6	–C=C– stretch	Alkenes
1762.82	C=O stretch	carbonyls (general)
2360.71	C≡N stretch	Nitriles
2737.77	H–C=O: C–H stretch	Aldehydes
3417.63	O–H stretch, H–bonded	alcohols, phenols
3547.81	O–H stretch, H–bonded	alcohols, phenols
3645.18	O–H stretch, free hydroxyl	alcohols, phenols

* Corresponding author: moslehali@ub.edu.sa, mabomughaid@gmail.com
0030-9923/2024/0001-0001 \$ 9.00/0



Copyright 2024 by the authors. Licensee Zoological Society of Pakistan.

This article is an open access  article distributed under the terms and conditions of the Creative Commons Attribution (CC BY) license (<https://creativecommons.org/licenses/by/4.0/>).